Signatures of extra gauge bosons in the littlest Higgs model with T parity at future colliders

Qing-Hong Cao*

Department of Physics and Astronomy, University of California at Riverside, Riverside, California 92321, USA

Chuan-Ren Chen†

Department of Physics and Astronomy, Michigan State University, East Lansing, Michigan 48824, USA

(Received 30 July 2007; published 15 October 2007)

We study the collider signatures of a T-odd gauge boson W_H pair production in the littlest Higgs model with T parity (LHT) at Large Hadron Collider (LHC) and Linear Collider (LC). At the LHC, we search for the W_H boson using its leptonic decay, i.e. $pp \to W_H^+ W_H^- \to A_H A_H \ell^+ \nu_\ell \ell'^- \bar{\nu}_{\ell'}$, which gives rise to a collider signature of $\ell^+\ell'^- + \not{E}_T$. We demonstrate that the LHC not only has a great potential of discovering the W_H boson in this channel, but also can probe enormous parameter space of the LHT. Because of four missing particles in the final state, one cannot reconstruct the mass of W_H at the LHC. But such a mass measurement can be easily achieved at the LC in the process of $e^+e^- \to W_H^+ W_H^- \to A_H A_H W^+ W^- \to A_H A_H jjjj$. We present an algorithm of measuring the mass and spin of the W_H boson at the LC. Furthermore, we illustrate that the spin correlation between the W boson and its mother particle (W_H) can be used to distinguish the LHT from other new physics models.

DOI: 10.1103/PhysRevD.76.075007 PACS numbers: 12.60.Cn, 14.80.Cp

I. INTRODUCTION

It has been shown that the collective symmetry breaking mechanism implemented in little Higgs models [1] provides an interesting solution to the ''little hierarchy problem'' (also see [2,3] for recent review). The littlest Higgs model, a $SU(5)/SO(5)$ nonlinear sigma model proposed in Ref. [4], is one of the most economical and interesting models discussed in the literature. In the littlest Higgs model, the global symmetry $SU(5)$ is broken down to $SO(5)$ by a 5×5 symmetric tensor at the scale f. Simultaneously, the gauged $[SU(2) \times U(1)]_1 \times [SU(2) \times U(1)]_2$, a subgroup of $SU(5)$, is broken to the diagonal $SU(2)_W \times U(1)_Y$, a subgroup of $SO(5)$. A vectorlike quark, T_+, is introduced in the top sector to cancel the quadratic divergence contribution to Higgs boson mass from the standard model (SM) top quark loop. The low energy electroweak precision tests (EWPT), however, enforce the symmetry breaking scale f to be larger than about 4 TeV. As a result, the cutoff scale $\Lambda \sim 4\pi f$ becomes so large that the fine-tuning between the cutoff scale and the electroweak scale is needed again [5–10]. The littlest Higgs model with T parity (LHT) [11–13] was proposed by imposing a discrete Z_2 symmetry, called T parity, into the Littlest Higgs model. T parity [11–13] is a symmetry which exchanges the gauge boson fields of the two gauged $SU(2) \times U(1)$ groups, i.e. $[SU(2) \times U(1)]_1 \leftrightarrow [SU(2) \times U(1)]_2$. One direct consequence of the T parity is the absence of the mixing between the extra heavy gauge bosons and the SM gauge bosons, because they have different T parity quantum numbers. The constraints from EWPT are alleviated so that the scale f could be as low as 500 GeV [14].

In order to incorporate the T parity systematically, extra fermion fields have to be introduced. One needs two sets of gauge boson fields and fermion fields transforming independently under $[SU(2) \times U(1)]_{1,2}$. One of the two possible linear combinations of the fields from two different sets is assigned to be the SM field and another combination is the extra heavy field. The heavy particles (except the vectorlike T_+) are odd under the T parity while the SM particles are even. With the exact T parity embedded, the effective operators which mix T-odd and T-even fields are absent. Details of the LHT considered in this paper have been shown in Refs. [15,16]. Here, we only lay out the mass spectrum of the particles relevant to our study, which are A_H (T parity partner of photon), W_H (T parity partner of W boson), ℓ_- (T-odd lepton) and q_- (T-odd quark),

$$m_{A_H} \simeq \frac{g' f}{\sqrt{5}}, \qquad m_{W_H} \simeq g f,$$
$$m_{\ell_-} \simeq \sqrt{2}\kappa_\ell f, \qquad m_{q_-} \simeq \sqrt{2}\kappa_q f,$$

where g' and g are the hypercharge and weak gauge coupling, respectively, and κ_ℓ (κ_q) is the Yukawa type coupling introduced in the interaction which generates the T-odd lepton (quark) mass. A_H is usually the lightest T-odd particle (LTP) which cannot further decay into the SM particles and thus plays as the dark matter candidate. With the allowed low mass scale, these extra T-odd particles have significant impacts on the phenomenology [17–33]. The Large Hadron Collider (LHC) at CERN has a great potential to copiously produce these new particles. Some studies about collider phenomenology of the LHT have been presented recently [15,16,21,34–37].

Current EWPT only impose constraints on the parameter space of the LHT. Because of the T parity, the new T-odd particles have to be produced in pairs at the colliders. The

*qcao@ucr.edu
†crchen@pa.msu.edu

fact that at least two missing particles remain in the final state makes it difficult to measure the model parameters of the LHT, see details in the discussions of the LHC phenomenology. In order to test the LHT at the LHC, one has to observe the new physics signatures in various independent channels. By comparing the model parameters extracted out from those channels one might be able to check the consistency of the LHT. For that, the $W_H^+ W_H^-$ production is of importance because the mass of the heavy gauge boson W_H (m_{W_H}) depends on f only. One thus can directly determine the symmetry breaking scale f from the W_H mass measurement.[1] In this paper, we examine the discovery potential of the $W_H^+ W_H^-$ pair production at the LHC and present a strategy of measuring the mass and spin of W_H at the LC. The matrix elements of both signal and background processes are calculated using MadGraph [38,39] while the widths of the new T-odd particles are calculated in CalcHEP [40] with the model file given by Ref. [16]. Agreement of both programs at the level of new gauge boson production has been checked. The rest of this paper is organized as follows. In Sec. II, we present the cross sections of the $W_H^+ W_H^-$ pair production at the LHC and at the LC. We also discuss the decay pattern of W_H and present the unitarity constraints on the parameter space of the LHT from effective four-fermion interaction operators. The collider phenomenology of the LHC and the LC is shown in Secs. III and IV, respectively. Finally, we conclude in Sec. V.

II. PRODUCTION AND DECAY OF W_H BOSON

The tree-level diagrams for a W_H pair production are shown in Fig. 1, where F and F' denote the quarks at the LHC while the electron and electron-neutrino at the LC. The W_H boson pair can be produced either via the s-channel process with the photon and Z boson exchanged or via the t-channel process with a T-odd fermion exchanged. Since the t-channel diagram involves the heavy T-odd fermion, its contribution depends on both m_{W_H} and m_{F_-}. In this work we choose the model parameters $(f, \kappa_{q/\ell})$ instead of the physical masses of the new particles as the theoretical inputs.

A. W_H production at the LHC

In Figs. 2(a) and 2(b) we show the total cross section of the W_H pair production as a function of κ_q and f, respectively. The T-odd quark in the t-channel diagram affects the total cross section significantly: (i) for 500 GeV $< f <$ 1000 GeV, there exists a $\kappa_q^{\min}(\sim 0.6)$ which minimizes the total cross section; (ii) for a fixed κ_q, the cross section decreases rapidly with increasing f. In order to understand why the minimum of the total cross section occurs, we separate the total cross section into three pieces,

$$\sigma_{\text{tot}} = \sigma_s + \sigma_t + \sigma_{\text{int}}, \tag{1}$$

where σ_s, σ_t, and σ_{int} denote the contributions of the s-channel diagram, t-channel diagram, and the interference between the s- and t-channel diagrams, respectively. For illustration, we choose $f = 500$ GeV and plot each individual contribution in Fig. 2(c). The s-channel diagram involves the gauge bosons only, therefore, its contribution depends on f but not on κ_q, cf. the flat blue curve. On the contrary, the t-channel contribution decreases with increasing κ_q, because the mass of the T-odd quark in the t-channel propagator grows with increasing κ_q, cf. the red curve. Although the s-channel and t-channel contributions are both constructive, their interference is destructive. The total cross section reaches the minimum when $\kappa_q \sim \kappa_q^{\min}$, where the s- and t-channel contributions are comparable. When $\kappa_q > \kappa_q^{\min}$, the total cross section is dominated by the s-channel contribution, therefore it drops rapidly with increasing f since the s-channel contribution suffers from the $1/\hat{s}$ suppression ($\hat{s}$ is the invariant mass of the W_H boson pair). When $\kappa_q \gg \kappa_q^{\min}$, the total cross section approaches to the s-channel contribution and both the t-channel contribution and the interference effect are negligible.

B. W_H production at the LC

We present the total cross section of the W_H pair production at the LC as a function of κ_ℓ and f in Figs. 3(a) and 3(b), respectively. In analogue to the W_H pair production at the LHC, there also exists a $\kappa_\ell^{\min}$ due to the destructive interference effect, but $\kappa_\ell^{\min}$ is very sensitive to f at the LC. As shown in Fig. 3(a), $\kappa_\ell^{\min}$ shifts from about 0.5 to 1.0 when f increases from 500 GeV to 750 GeV. We also note that the total cross section of a small κ_ℓ, e.g. $\kappa_\ell = 0.3$, drops much slower than the total cross section of a large κ_ℓ, see Fig. 3(b).

Following the LHC study, we split the total cross section into the s-channel, t-channel and the interference contributions. In Fig. 4 we explicitly plot the total cross section (black curve), the s-channel contribution (blue curve), the t-channel contribution (red curve), and the interference contribution (green curve). Figures 4(a) and 4(b) show the total cross section as a function of κ_ℓ for $f =$ 500 GeV and 750 GeV, respectively. We have learned from the LHC study that the minimal cross section for a fixed f occurs when $\sigma(s) \simeq \sigma(t)$. When f increases from 500 GeV to 750 GeV, the s-channel contribution drops rapidly since it suffers from the $1/\hat{s}$ suppression, but on the other hand, the t-channel contribution does not. Of course, increasing the f value will increase the mass of the W_H boson and reduce the t-channel contribution, but the sup-

[1] Recently, Ref. [21] proposed that one can measure f using the spin correlation between the top quark pair in the process of $pp \to T_- T_- \to t A_H \bar{t} A_H$, where T_- is the T parity partner of the vectorlike T_+.

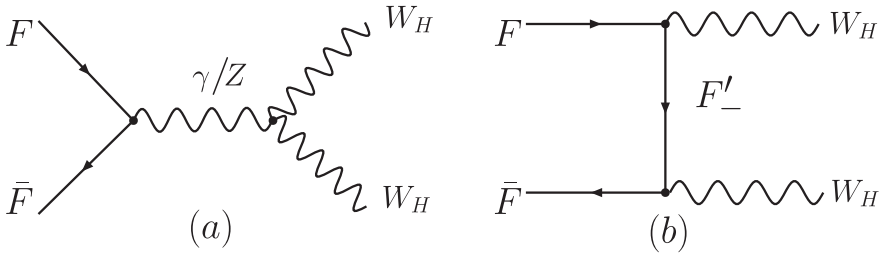

FIG. 1. Feynman diagrams for a W_H pair production.

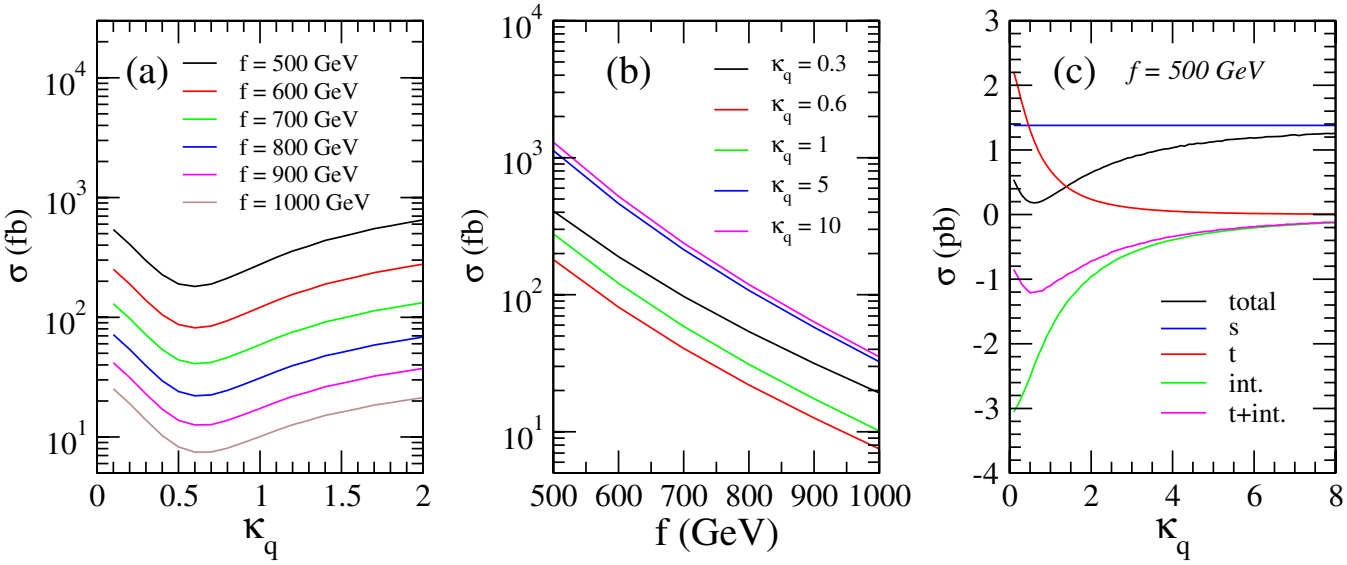

FIG. 2 (color online). The total cross section of a $W_H^+W_H^-$ pair production at the LHC for various parameters f and κ_q.

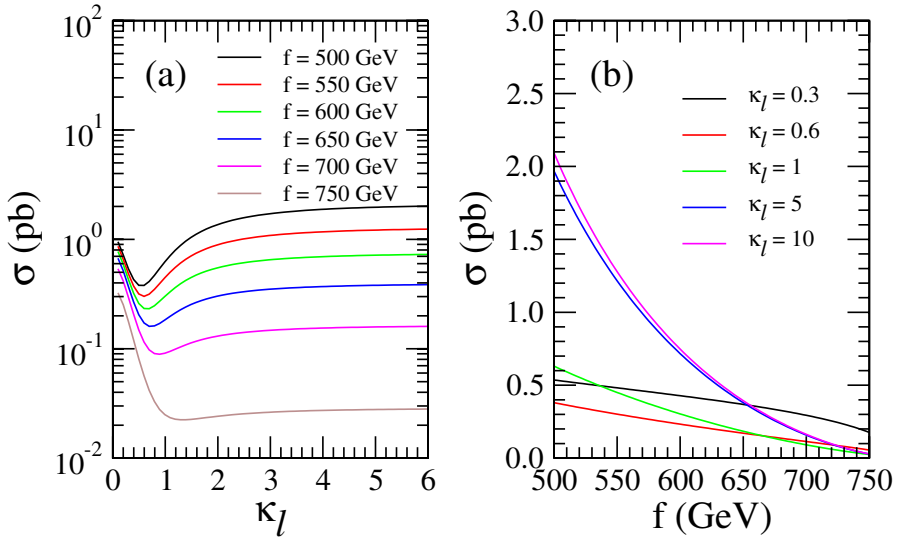

FIG. 3 (color online). Total cross section of a $W_H^+W_H^-$ pair production at the LC for various f and κ_ℓ.

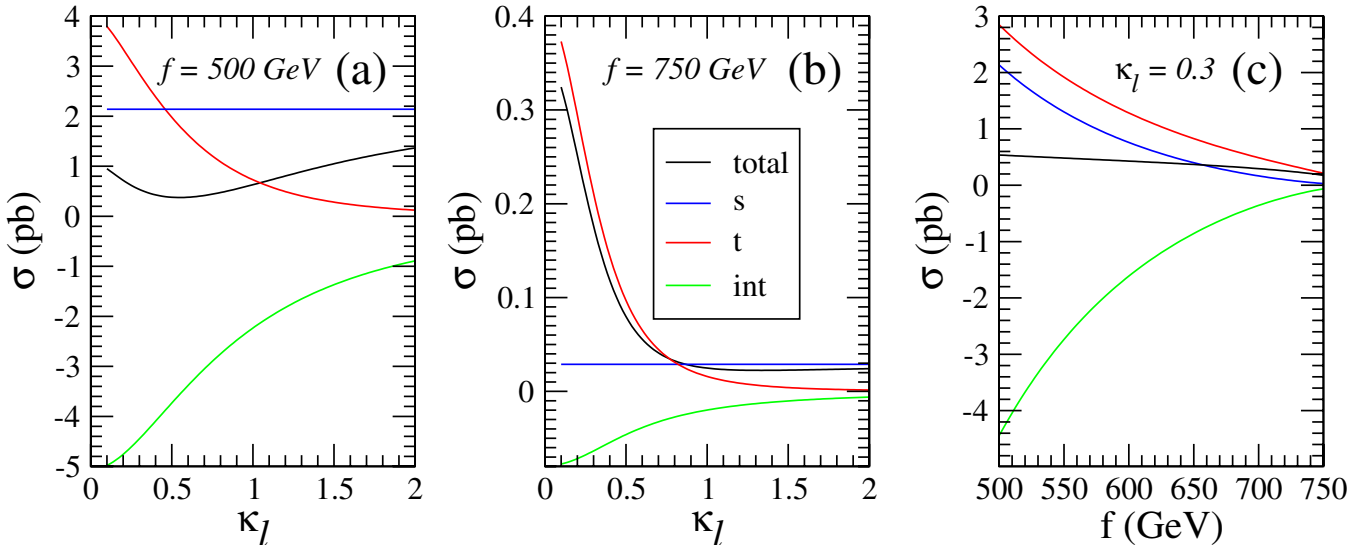

FIG. 4 (color online). The distributions of s-, t-channel diagrams and interference term in the $W_H^+ W_H^-$ production at the LC.

pression in the t-channel contribution is much less than that in the s-channel contribution. Therefore, the position for $\sigma(s) \simeq \sigma(t)$ is shifted to the larger κ_ℓ region. The reason why the cross section of $\kappa_\ell = 0.3$ drops slowly in the large f region can also be understood from the competition between the s- and t-channel contributions. In Fig. 4(c) we show the total cross section as a function of f for $\kappa_\ell = 0.3$. For such a small κ_ℓ, the T-odd neutrino's mass is small ($m_{\nu_-} \simeq 0.42f$). Then the t-channel contribution dominates over the s-channel contribution. In the large f region, i.e. 600 GeV $< f <$ 750 GeV, the s-channel contribution as well as the interference effect both decrease to zero, and the total cross section approaches to the t-channel contribution which does not drop rapidly with increasing f.

C. Decay of the W_H boson

The W_H boson will decay into a T-odd particle and a T-even SM particle. Its decay pattern is mainly determined by the masses of new T-odd particles. In the LHT,

$$\begin{aligned} m_{A_H} &\simeq \frac{g' f}{\sqrt{5}} \simeq 0.156 f, \\ m_{W_H} &\simeq g f \simeq 0.653 f, \\ m_{\ell_-} &\simeq \sqrt{2}\kappa_\ell f \simeq 1.414 \kappa_\ell f, \\ m_{q_-} &\simeq \sqrt{2}\kappa_q f \simeq 1.414 \kappa_q f. \end{aligned} \tag{2}$$

It is clear that the A_H boson is always lighter than the W_H boson. But the T-odd quark (lepton) can be heavier or lighter than the W_H boson, depending on the parameter $\kappa_q(\kappa_\ell)$. Let us denote F_- as the T-odd fermion whose mass m_{F_-} is $\sqrt{2}\kappa f$. When $\kappa < 0.11$, $m_{F_-} < m_{A_H} < m_{W_H}$; therefore, the T-odd lepton or T-odd quark will play the role as the dark matter candidate. As pointed out in Ref. [41], the dark matter candidates should be charge neutral and colorless objects. Hence, we focus our attention to the case of $\kappa_\ell(\kappa_q) > 0.11$ throughout this study, i.e. demanding A_H to be the lightest T-odd particle. When both κ_q and κ_ℓ are larger than 0.462, i.e. $m_{A_H} < m_{W_H} < m_{F_-}$, the W_H boson only decays via the $W_H \to W + A_H$ channel. When $0.11 < \kappa < 0.462$, i.e. $m_{A_H} < m_{F_-} < m_{W_H}$, then the W_H boson can decay into either WA_H or $F_- F'$ (F' being the usual SM fermion).

In Fig. 5(a) we summarize the decay pattern of W_H in the plane of κ_q and κ_ℓ, where the following decay modes are considered:

$$W_H \to W A_H \to \ell \bar{\ell}' (q \bar{q}') A_H, \tag{3}$$

$$W_H \to \ell_- \nu_\ell \to \ell A_H \nu_\ell, \tag{4}$$

$$W_H \to \nu_{\ell_-} \ell \to \nu_\ell A_H \ell, \tag{5}$$

$$W_H \to q_- q' \to q A_H q'. \tag{6}$$

Here, $\ell(\nu, q)$ denotes the charged leptons (neutrinos, quarks). We also include the subsequent decay of the second T-odd fermions whose decay branching ratio is 100% for $0.11 < \kappa < 0.462$. In the above decay modes, the $W_H \to t b_- \to t b A_H$ mode is special because of large top quark mass (m_t). In order to open the decay mode $W_H \to t b_-$, the mass constraint $m_{W_H} > m_t + m_{b_-}$ has to be satisfied and the allowed region of κ_q and f is shown in Fig. 5(b). As shown in Eq. (2), the mass relation between the W_H, A_H, and F_- is fixed by κ and does not depend on f. Thus, the decay branching ratios of the $W_H \to W A_H$ and $W_H \to F_- F'$ modes do not depend on f if the $t b_-$ mode is not opened. Once the $t b_-$ mode is opened, the decay branching ratios of other modes will be slightly reduced. In Fig. 6 we show the decay branching ratios of the W_H

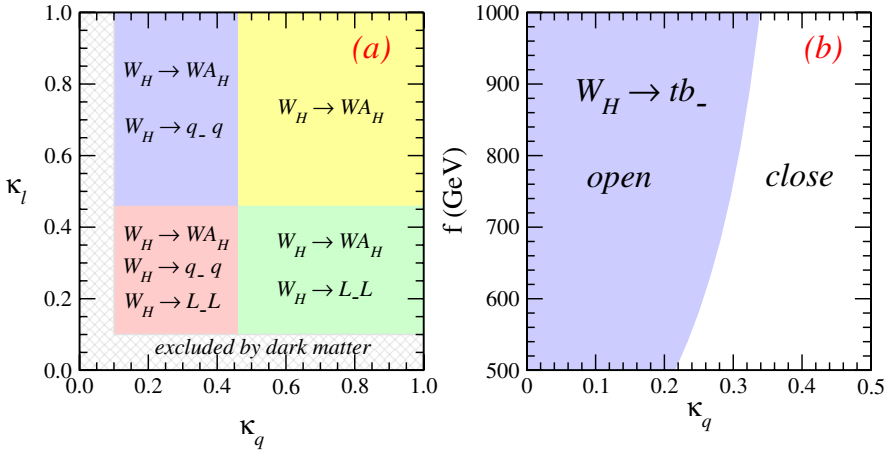

FIG. 5 (color online). (a) Pictorial illustration of the decay pattern of the W_H boson in the plane of κ_ℓ and κ_q; (b) allowed region (blue) of κ_q for the $W_H \to tb\_$ mode being opened.

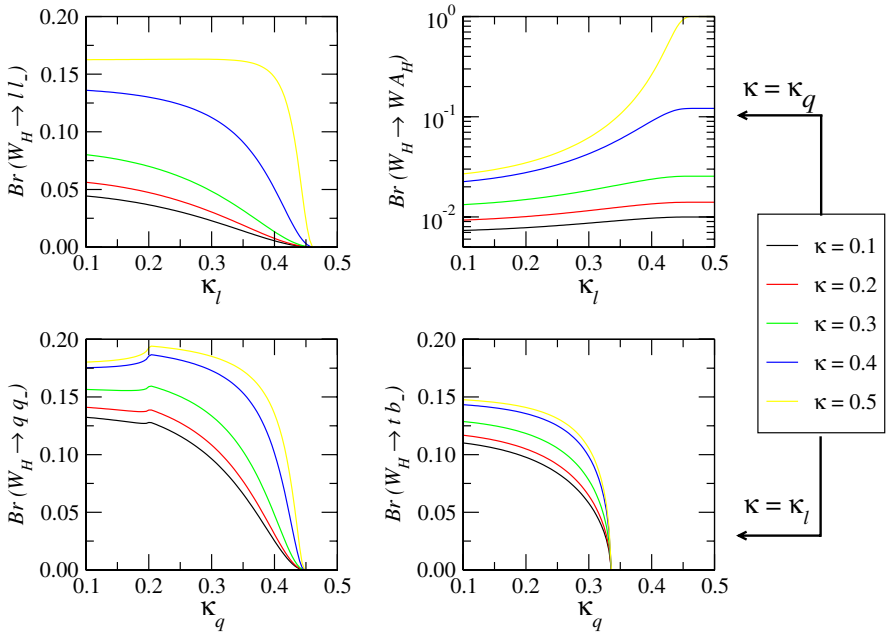

FIG. 6 (color online). Decay branching ratios of the W_H boson for $f = 500$ GeV.

TABLE I. Decay branching ratios (%) of the W_H boson for a few benchmark points, where $\ell = e, \mu, \tau$, $\nu = \nu_e, \nu_\mu, \nu_\tau$, $U = u, c$ and $D = d, s$. Note that all the SM fermions (except the top quark) are treated as massless.

	$\kappa_\ell = 0.3$ $\kappa_q = 0.3$			$\kappa_\ell = 0.5$ $\kappa_q = 0.3$			$\kappa_\ell = 0.3$ $\kappa_q = 0.5$			$\kappa_\ell = 0.5$ $\kappa_q = 0.5$
f (GeV)	500	700	1000	500	700	1000	500	700	1000	>500
ℓ_ν	4.45	4.61	4.33	0	0	0	15.0	15.9	16.3	0
ν_ℓ	4.84	4.81	4.41	0	0	0	16.3	16.5	16.6	0
U_D	14.5	14.4	13.2	20.1	20.1	17.9	0	0	0	0
D_U	13.4	13.8	13.0	18.5	19.3	17.6	0	0	0	0
t_b	14.5	14.4	13.2	20.1	20.1	17.9	0	0	0	0
$tb\_$	0	0	7.79	0	0	10.6	0	0	0	0
WA_H	1.84	0.8	0.33	2.55	1.12	0.45	6.19	2.76	1.25	100

boson as a function of κ_ℓ and κ_q, respectively. Explicit numbers of the decay branching ratios for the selected benchmark points are listed in Table I.

D. Unitarity constraints on κ_q and κ_ℓ

Let us examine the low energy constraints on κ_ℓ and κ_q in this section before studying the phenomenology of the W_H boson. The mass constraints on T-odd fermions, i.e. the lepton (ℓ_-) and quark (q_-), could be derived from four-fermion interaction operators $O(ffff)$.

The most general chirally invariant form of the four-fermion interaction reads

$$\frac{g^2}{2\Lambda^2}\bar{\psi}_L\gamma^\mu\psi_L\bar{\psi}_L\gamma_\mu\psi_L,$$

where Λ is the new physics scale. One then can determine the scale Λ unambiguously from the unitarity condition by setting $g^2(\Lambda)/4\pi = 1$ for the new strong interaction coupling. For example, $\Lambda(eeee) > 10.3$ TeV, $\Lambda(eedd) > 26.4$ TeV, and $\Lambda(uudd) > 2.4$ TeV at 95% confidence level [42]. Using these limits, we can calculate the upper bound on T-odd fermion masses. If we assume the universal mass for T-odd lepton (ℓ_-) and quark (q_-), i.e. $\kappa_\ell = \kappa_q = \kappa$, the strongest constraint is from $O(eedd)$ [14], which leads to

$$\kappa_\ell = \kappa_q \leq 3.4\frac{f}{\text{TeV}}. \tag{7}$$

However, there is no physics reason to believe that the lepton and quark sectors will share the same κ. In this work we will treat κ_ℓ and κ_q separately. As a result, the masses of the T-odd leptons differ from the masses of the T-odd quarks. In order to avoid the problem of flavor changing neutral current, we further assume κ_ℓ and κ_q are universal individually and also diagonal in the flavor space. Under this assumption, we obtain the constraints on κ_ℓ and κ_q separately from $O(eeee)$ and $O(uudd)$ as follows:

$$\kappa_\ell \leq 8.6\frac{f}{\text{TeV}}, \tag{8}$$

$$\kappa_q \leq 37.1\frac{f}{\text{TeV}}. \tag{9}$$

However, κ_q and κ_ℓ are correlated by the $O(eedd)$ which leads to

$$\frac{\kappa_\ell^2\kappa_q^2}{\kappa_\ell^2 - \kappa_q^2}\ln\left(\frac{\kappa_\ell}{\kappa_q}\right) \leq \frac{128\pi^3 f^2}{(26.4\text{ TeV})^2}. \tag{10}$$

Figure 7 shows the correlation of Eq. (10) for various values of f. The region below each curve is the allowed parameter space of κ_ℓ and κ_q for the corresponding f. The constraint is tight for small f: when $f = 500$ GeV, large κ_q prefers smaller κ_ℓ and vice versa, for example, $\kappa_q > 4$ requires $\kappa_\ell < 1$. This constraint becomes quite loose when f becomes large.

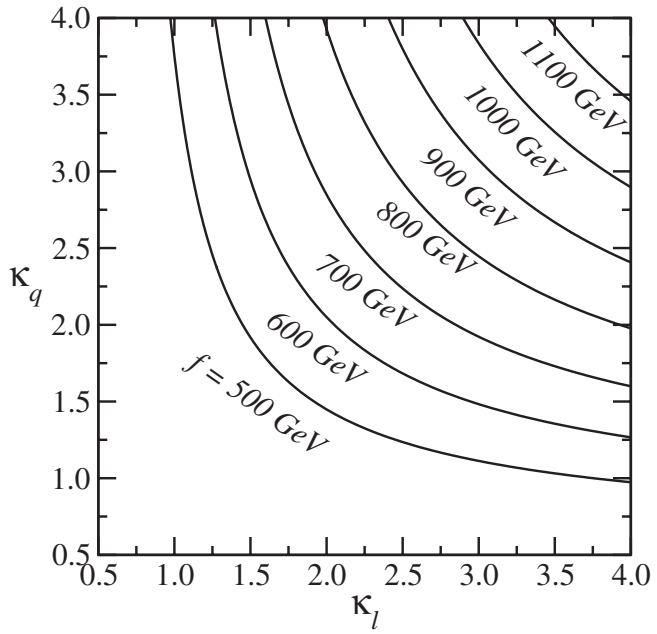

FIG. 7. Allowed region of κ_ℓ and κ_q for various values of f. The region below each curve is allowed.

III. PHENOMENOLOGY OF THE W_H PAIR PRODUCTION AT THE LHC

The production rate of $W_H^+W_H^-$ pair at the LHC is sizable, but the detection for its signatures at the hadron collider was expected to be challenging [15,16]. However, in this work we will demonstrate that the LHC not only has a great potential to discover the collider signature of the $W_H^+W_H^-$ pair production, but also has the capability to explore enormous parameter space of f and κ. Below we present a detailed study of the LHC phenomenology.

At the LHC, we demand the two W_H bosons both decay leptonically in order to avoid the huge QCD backgrounds. We further require the two charged leptons in the final state having different lepton flavors. Hence, the collider signature of the signal events is $e^+\mu^-\not{E}_T$ (or $e^-\mu^+\not{E}_T$), where the missing energy ($\not{E}_T$) is originated from two A_H's and two neutrinos. For simplicity, we will present the study of $e^+\mu^-\not{E}_T$ signature throughout this paper, but it is very straightforward to include the contribution of $e^-\mu^+\not{E}_T$ mode as those two decay modes are identical.[2]

When W_H is the second lightest T-odd particle, i.e. κ_q and κ_ℓ are both larger than 0.462, the signal events only come from the following process:

[2]The mass difference between e and μ can be safely ignored in our study since we are dealing with new particles whose masses are at the order of TeV.

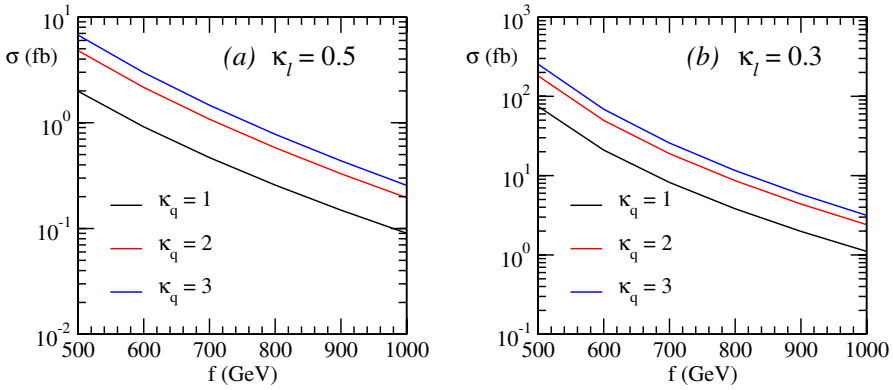

FIG. 8 (color online). The total cross section of $pp \to W_H^+ W_H^- \to e^+ \mu^- \not{E}_T$ at the LHC.

$$pp \to W_H^+ W_H^- \to A_H W^+ (\to e^+ \nu_e) A_H W^- (\to \mu^- \bar{\nu}_\mu). \tag{11}$$

However, when the T-odd leptons are lighter than W_H, i.e. $\kappa_\ell < 0.462$, the signal will mainly come from the process

$$pp \to W_H^+ W_H^- \to \ell_{1-} \ell_2 \ell_{3-} \ell_4 \to e^+ \mu^- \nu_e \bar{\nu}_\mu A_H A_H, \tag{12}$$

where $\ell_i = e$, μ, ν_e, or ν_μ. The total cross sections of these two processes are shown in Fig. 8 where the left plot is for the process in Eq. (11) with $\kappa_\ell = 0.5$ while the right plot is for the process in Eq. (12) with $\kappa_\ell = 0.3$. If W_H is the second lightest T-odd particle, the signal will only come from Eq. (11) since the W_H can only decay to WA_H; otherwise, the process in Eq. (12) dominates. The total rate of the signal events depends on the masses of ℓ_-, q_-, and W_H, and as shown in Fig. 8, the total cross section is sizable when f is small and κ_q is large. This is because the mass of the T-odd gauge boson is light and the destructive effect from t-channel and s-channel interference term is small.

The main intrinsic backgrounds come from the W^+W^- and the ZW^+W^- continuum productions with the subsequent decays $W^+ \to \ell^+ \nu_\ell$, $W^- \to \ell^- \bar{\nu}_\ell$, and $Z \to \nu\nu$.[3] There also exist other reducible backgrounds from the top quark pair production and the Wt associated production which can be highly suppressed by vetoing the additional b-jet from the top quark decay with large transverse momentum or in the central rapidity region. The vetoing efficiency is so large, about 99.9% for the $t\bar{t}$ background and 99.6% for the Wt background, that we only need to consider the intrinsic backgrounds in this study. The total cross section of the W^+W^- pair production background is about 0.865 pb while the other intrinsic background from W^+W^-Z is negligible (~ 0.08 fb). These cross sections already include the decay branching ratios of $W \to \ell\nu$ and $Z \to \nu\nu$. Below, we just consider the W^+W^- pair production as the background at the LHC.

Kinematics of the signal events is distinctively different from that of background events. As to be shown later, these differences can be used to significantly suppress the background and enhance the ratio of signal to background (S/B). For illustration, we show normalized distributions of various kinematics observables of the signal and background events in Fig. 9: transverse momentum ($p_T^{e/\mu}$), rapidity ($\eta^{e/\mu}$), energy ($E^{e/\mu}$) of charged leptons, invariant mass of two charged leptons ($m_{e\mu}$), missing transverse momentum ($\not{E}_T$) and cosine of the opening angle between two charged leptons ($\cos\theta_{e\mu}$). The curves labeled by $\kappa_\ell = 0.5$ and $\kappa_\ell = 0.3$ correspond to the signals described in Eq. (11) and (12), respectively. A few interesting points are summarized below:

(i) Compared to the background, the typical feature of the signal events is that the final state particles are more energetic, cf. Figs. 9(a) and 9(c)–9(e).

(ii) As the decay products of heavy W_H bosons, the two charged leptons mainly appear in the central region, cf. Fig. 9(b), because W_H is hardly boosted.

(iii) We also note that, unlike the background, two charged leptons of the signal do not exhibit strong correlations, see the nearly flat behavior in the $\cos\theta_{e\mu}$ distribution. It can be understood as follows. Since m_{W_H} is much larger than m_W and m_{A_H}, W and A_H will be predominately in the longitudinal polarization state, i.e. behaving as scalars. Thus, the spin correlation between e^+ and μ^- is lost, which results in a flat distribution. On the contrary, the two charged leptons in the SM background are highly correlated.

(iv) The signal distributions change a lot when varying the value of κ_ℓ. In particular, for a Small κ_ℓ, i.e. $\kappa_\ell = 0.3$, the peak positions of the $p_T^{e/\mu}$, $m_{e\mu}$, $E_e^{e/\mu}$, and $\not{E}_T$ distributions are shifted to the large

[3]Generally speaking, we also need to consider the background from the Higgs boson decay into a W boson pair, which is $gg \to H \to W^+W^-$. The total rate depends on the mass of Higgs boson. For instance, the total cross section is ~95 fb when the Higgs boson is 120 GeV, and ~230 fb when Higgs boson is 170 GeV. However, it can be completely suppressed by imposing the kinematics cuts discussed later.

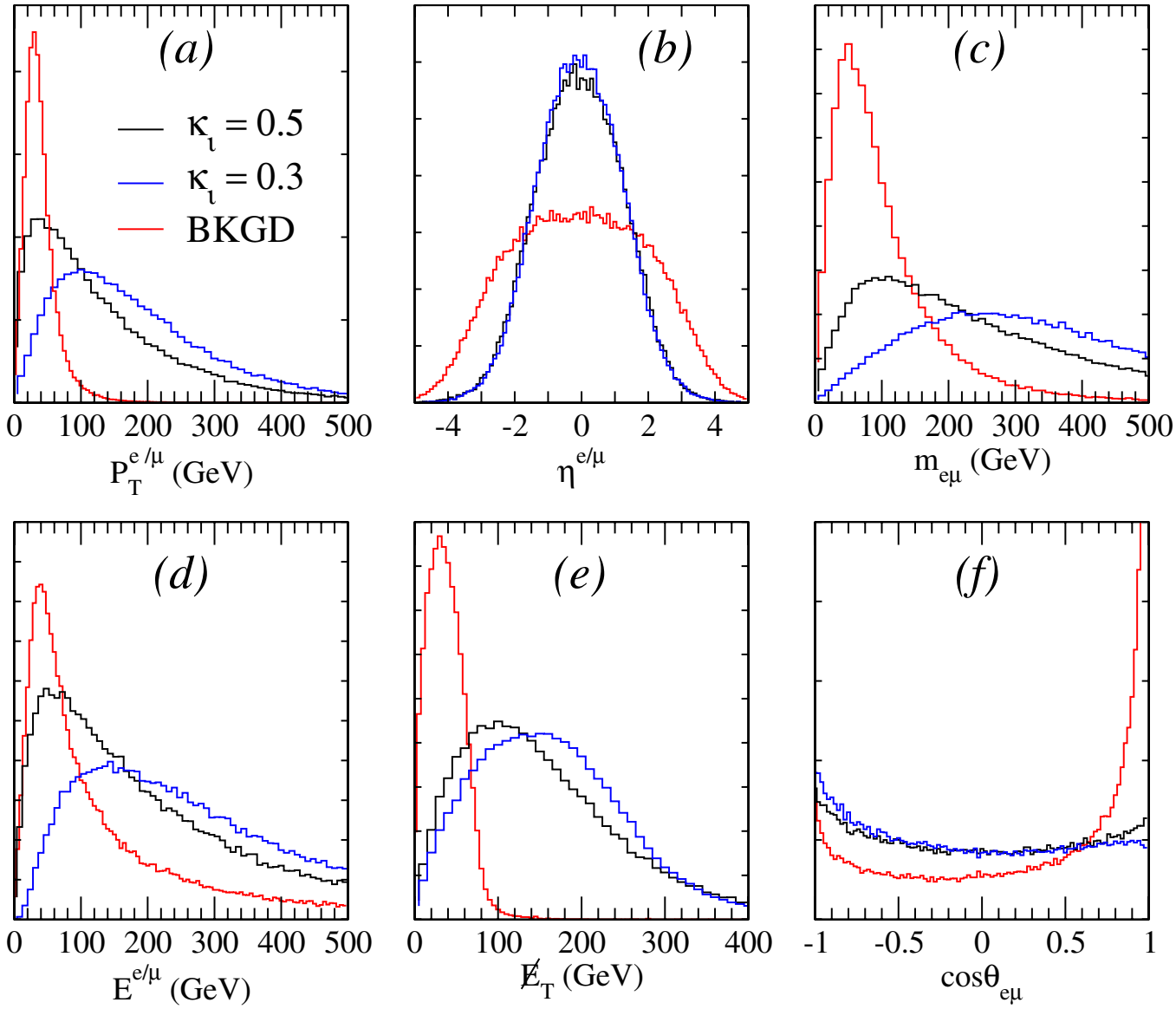

FIG. 9 (color online). Transverse momentum of e^+/μ^- ($p_T^{e/\mu}$), rapidity of e^+/μ^- ($\eta^{e/\mu}$), invariant mass of e^+ and μ^- ($m_{e\mu}$), energy of e^+/μ^- ($E^{e/\mu}$), missing transverse momentum ($\not{E}_T$), cosine of the opening angle between e^+ and μ^-($\cos\theta_{e\mu}$) distributions for $\kappa_q = 1$ and $f = 700$ GeV. All curves are normalized by their total cross sections.

value region when compared to those of large κ_ℓ, i.e. $\kappa_\ell = 0.5$. This is due to the fact that for a small κ_ℓ, the charged leptons (e^+ and μ^-) or the neutrinos (ν_e and $\bar{\nu}_\mu$) are directly generated from the W_H boson decay, e.g. $W_H^+ \to e^+\nu_{e_-}$ or $W_H^+ \to \nu_e e^+_-$, and therefore are more energetic.

In order to mimic the detector, we require $p_T^{e/\mu}$ and $\eta^{e/\mu}$ to satisfy the following basic cuts:

$$p_T^e > 20.0 \text{ GeV}, \qquad p_T^\mu > 20.0 \text{ GeV}, \qquad |\eta^e| < 2.0, \qquad |\eta^\mu| < 2.0. \tag{13}$$

Furthermore, taking advantage of the differences between the kinematics of the signal and background events, we impose the following *optimal cuts* to extract the signal out of the SM background,

$$\not{E}_T > 175 \text{ GeV}, \qquad \cos\theta_{e\mu} < 0.6. \tag{14}$$

After imposing the optimal cuts, the main background from the W^+W^- pair production can be suppressed by more than 99% and gives rise to 18 background events for $\mathcal{L} = 10$ fb^{-1} while 192 events for $\mathcal{L} = 100$ fb^{-1}, where $\mathcal{L}$ denotes the integrated luminosity. These background rates include both $e^+\mu^-$ and $e^-\mu^+$ modes. In Fig. 10 we present the 5σ, 3σ statistical significance and 95% confidence level (C.L.) for $\kappa_\ell = 0.5$ (top row) and $\kappa_\ell = 0.3$ (bottom row). For $\kappa_\ell = 0.5$, the W_H boson is the second lightest T-odd particle and the signal events come

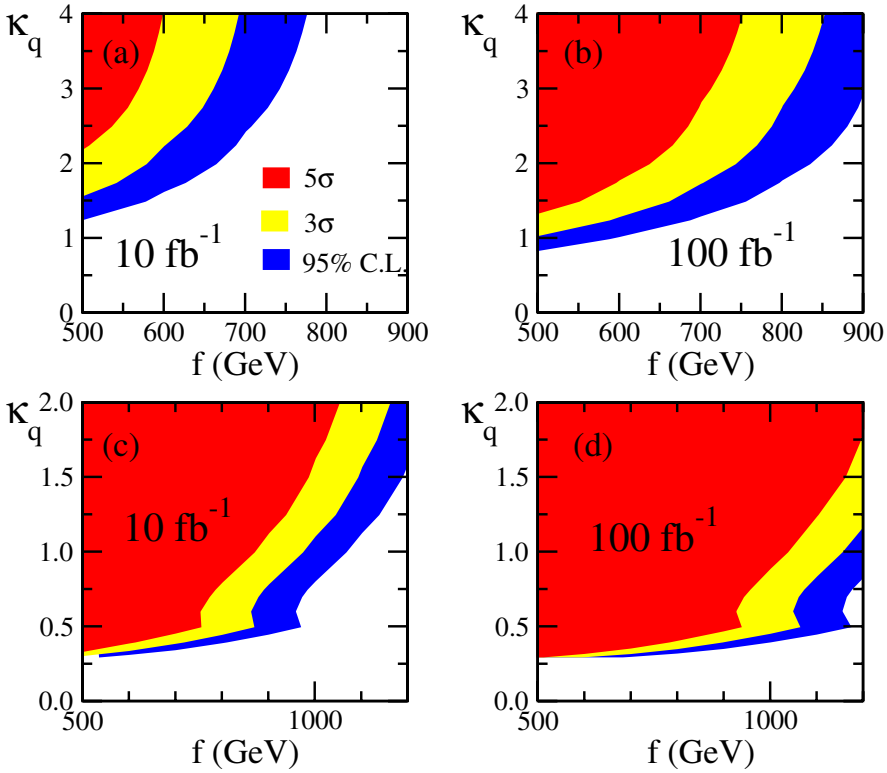

FIG. 10 (color online). Statistical significance contour of signature of $pp \to W_H^+ W_H^- \to \ell^+ \ell'^- \nu_\ell \bar{\nu}_{\ell'} A_H A_H$ in the plane of κ_q and f at the LHC. The upper two plots are for $\kappa_\ell = 0.5$ while the lower two are for $\kappa_\ell = 0.3$.

from Eq. (11) only. When f is 500 GeV, the signal can reach more than 3σ statistical significance for $\kappa_q \gtrsim 1.5$ with $\mathcal{L} = 10$ fb^{-1} and $\kappa_q \gtrsim 1$ with $\mathcal{L} = 100$ fb^{-1}, respectively. Furthermore, the f can be probed up to about 770 GeV with $\mathcal{L} = 10$ fb^{-1} and 950 GeV with $\mathcal{L} = 100$ fb^{-1}, respectively, at the 95% C.L. On the other hand, for $\kappa_\ell = 0.3$, the T-odd leptons are lighter than W_H and the signal events predominantly come from Eq. (12) due to the large decay branching ratios. In this case, one can probe more parameter space of the LHT, cf. Fig. 10(c) and 10(d). For example, assuming $\kappa_q = 1$, one can probe f up to 900 GeV with $\mathcal{L} = 10$ fb^{-1} and 1050 GeV with $\mathcal{L} = 100$ fb^{-1}, respectively, at the 5σ level.

As shown above, it is very promising to use the $e\mu + \not{E}_T$ signature to detect the $W_H W_H$ pair production at the LHC.

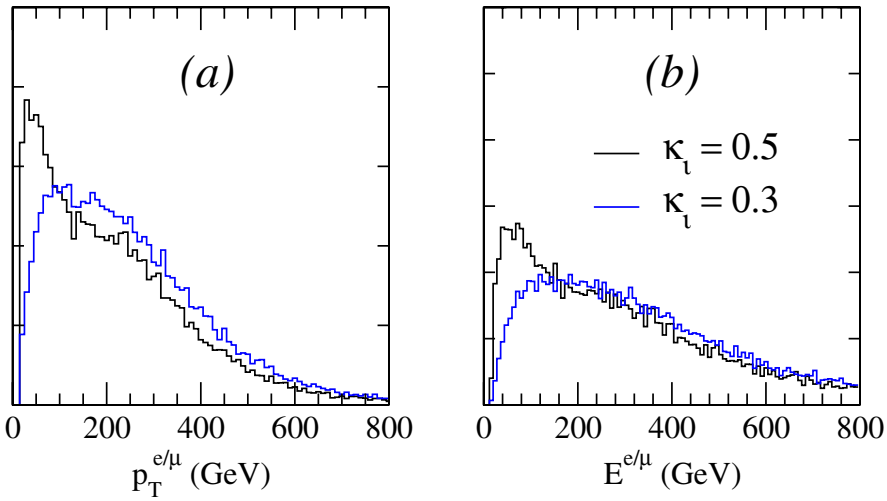

FIG. 11 (color online). Normalized distributions of $p_T^{e/\mu}$ and $E^{e/\mu}$ for $f = 700$ GeV and $\kappa_q = 1$ for $pp \to W_H^+ W_H^- \to e^+ \mu^- \nu_e \bar{\nu}_\mu A_H A_H$ process after imposing the kinematics cuts given in Eq. (14) at the LHC.

But such a signature can originate from two processes, either Eq. (11) or Eq. (12), depending on the value of κ_ℓ. Therefore, one immediate task after observing such a signature is to determine from which process it comes. It turns out that this question can be easily answered by the $p_T^{e/\mu}$ and $E^{e/\mu}$ distributions, cf. Fig. 11 where we have imposed the optimal cuts. In case of $\kappa_\ell = 0.3$, the charged lepton is directly emitted from the T-odd gauge boson decay, therefore its transverse momentum is typically larger than the one of the charged lepton emitted form the W-boson decay, i.e. $\kappa_\ell = 0.5$. The same argument also works for the energy distributions. Hence, one can fit the observed $p_T^{e/\mu}$ and $E^{e/\mu}$ distributions to the LHT predictions to measure κ_ℓ, though κ_q remains unknown as it merely changes the normalization of both distributions.

IV. PHENOMENOLOGY OF THE W_H PAIR PRODUCTION AT THE LC

Compared to the LHC, the LC does not have sufficient energy to produce very heavy W_H bosons. For example, the LC can only probe the W_H boson mass up to 500 GeV, which corresponds to $f \simeq 750$ GeV. However, the LC provides a much cleaner experimental environment (no QCD backgrounds) which is perfect for precision measurements. As mentioned before, because of suffering from the extremely huge QCD backgrounds, one has to use the leptonic decay mode for the W_H boson search at the LHC. One can observe a deviation from the SM prediction, but one cannot determine the mass or spin of the W_H boson due to the four missing particles (two A_H's and two neutrinos) in the final state. In this section we preform a comprehensive study of the W_H pair production at the LC and address the following questions:

(i) Can one determine the masses of W_H and A_H?
(ii) Can we reconstruct the kinematics of the missing particle A_H?
(iii) Can we measure the spin of W_H?

As will be shown later, all these questions can be easily answered at the LC with the help of the known center-of-mass energy.

At the LC, we are able to search the W_H boson using its hadronic decay mode $W_H \to A_H W \to A_H jj$. Below, we consider the following signal process:

$$e^+e^- \to W_H^+ W_H^- \to W^+(\to jj)W^-(\to jj)A_H A_H, \quad (15)$$

which gives rise to a collider signature of four isolated jets associated with large missing energy originated from the two undetectable A_H bosons in the final state. The main intrinsic background is from the process $e^+e^- \to W^+W^-Z \to jjjj\nu\bar{\nu}$ whose cross section is about 5.6 fb. In Fig. 12, we show the cross section of the signal process given in Eq. (15) at the LC. The total cross section relies on how large the decay branching ratio of the $W_H \to WA_H$ mode is (1) when both κ_ℓ and κ_ℓ are large, $\mathrm{Br}(W_H \to WA_H) = 1$ which leads to a large cross section, see the solid (black) curve; (2) when either κ_q or κ_ℓ is small, $\mathrm{Br}(W_H \to WA_H)$ is highly suppressed, so the total cross section becomes small; see the dashed (blue), the dotted (red), and the dotted-dashed (green) curves. In this work we focus our attention on the first case, i.e. large κ_q and κ_ℓ, in which W_H is the second lightest T-odd particle. Since the cross section of the signal process is much higher than the WWZ background, it is not difficult to disentangle the signal from the background. Therefore, only the basic kinematics cuts, but no further hard cuts, are applied to select the event in the following study. For comparison, we also present the background distributions.

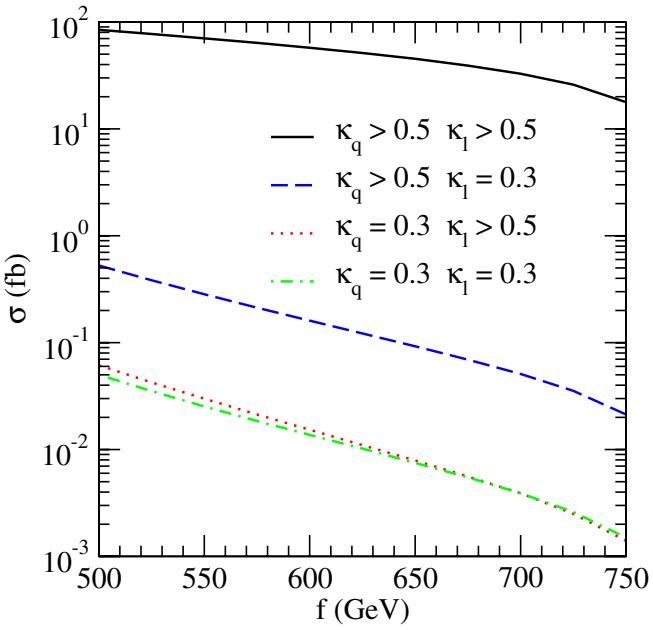

FIG. 12 (color online). Total cross section for $e^+e^- \to W_H^+W_H^- \to A_H A_H jjjj$ at the LC.

When either κ_q or κ_ℓ is small, one has to consider other decay modes to search the W_H boson. For example, when $\kappa_q = 0.3$, the T-odd quark is lighter than the W_H boson. One thus can use the following process

$$e^+e^- \to W_H^+W_H^- \to qq'_-qq'_- \to qqqqA_HA_H \quad (16)$$

to search the W_H boson. Searching the W_H boson in this channel is very interesting but certainly beyond the scope of this work. Detailed study of this channel will be presented elsewhere.

A. Mass measurement of W_H

In order to simulate the detector acceptance, we require the transverse momentum (p_T^j) and rapidity (η^j) of all the final state jets to satisfy the following basic cuts:

$$p_T^j > 15 \text{ GeV}, \qquad |\eta^j| < 3.$$

We also demand that the four jets are resolvable as separated objects, i.e. requiring the separation in $\Delta R \equiv \sqrt{(\delta\eta)^2 + (\delta\phi)^2}$ between any two jets to be larger than 0.4, where $\delta\eta$ and $\delta\phi$ denotes the separation in the rapidity and azimuthal angles, respectively. In order to reconstruct the two W bosons, one needs to isolate the four jets coming from the W boson decay. Unfortunately, one cannot tell the jets apart experimentally because the information of quark's charge and flavor is lost in the hadronization of the light quarks. In order to measure m_{W_H}, one needs to reconstruct the two W bosons, i.e. finding out which two jets come from which W boson. In this study we use the W boson mass as a constraint to reconstruct two W bosons:

(i) In order to identify the jets, we order the four jets by their transverse momentum,

$$p_T^{j_1} \geq p_T^{j_2} \geq p_T^{j_3} \geq p_T^{j_4}. \quad (17)$$

(ii) We loop over all combinations of the four jets, i.e. (j_1j_2, j_3j_4), (j_1j_3, j_2j_4) and (j_1j_4, j_2j_3), and calculate the invariant masses of the reconstructed W bosons. We then calculate the deviations from the true W boson mass (m_W) for each combination,

$$\Delta = \sqrt{(m_1(jj) - m_W)^2 + (m_2(jj) - m_W)^2}, \quad (18)$$

and select the combination giving rise to the minimal deviations to reconstruct the W bosons. Although the efficiency of the W boson reconstruction procedure is very high ($\sim 99.1\%$), we cannot distinguish the two reconstructed W bosons because the charge information is lost. But as will be shown below, we do not need the information of the W boson charge to determine the mass and spin of W_H. Just for bookmark we denote the W boson consisting of the highest p_T jet as W_1 while the other W boson as W_2.

In Fig. 13, we present the energy distributions of the reconstructed W bosons (E_W) where the energy of W_1 (E_{W_1}) peaks in the large energy region while the energy of W_2 (E_{W_2}) in the small energy region. The asymmetry between W_1 and W_2 is due to our requirement that the W_1 boson includes the leading-p_T jet. Since the A_H bosons are massive, the E_W distributions exhibit sharp drops in both small and large energy regions, which can be used to measure the masses of W_H and A_H [43]. The ending points of the energy distribution of the W boson are given by

$$E_\pm = \gamma(E_W^\star \pm \beta p_W^\star), \quad (19)$$

where $\beta = \sqrt{1 - 4m_{W_H}^2/s}$, $\gamma = 1/\sqrt{1-\beta^2}$ and $E_W^\star(p_W^\star)$ is the energy (momentum) magnitude of the W boson in the rest frame of W_H,

$$E_W^\star = \frac{m_{W_H}^2 - m_{A_H}^2 + m_W^2}{2m_{W_H}}, \quad (20)$$

$$p_W^\star = \frac{\sqrt{[m_{W_H}^2 - (m_{A_H} + m_W)^2][m_{W_H}^2 - (m_{A_H} - m_W)^2]}}{2m_{W_H}}. \quad (21)$$

From $E_\pm$ we can derive m_{W_H} and m_{A_H} as follows:

$$m_{W_H} = \sqrt{\frac{s}{2}}\frac{\sqrt{E_+E_-}}{E_+ + E_-} \times \sqrt{1 + \frac{m_W^2}{E_+E_-} + \sqrt{\left(1 - \frac{m_W^2}{E_+^2}\right)\left(1 - \frac{m_W^2}{E_-^2}\right)}}, \quad (22)$$

$$m_{A_H} = m_{W_H}\sqrt{1 - \frac{2(E_+ + E_-)}{\sqrt{s}} + \frac{m_W^2}{m_{W_H}^2}}. \quad (23)$$

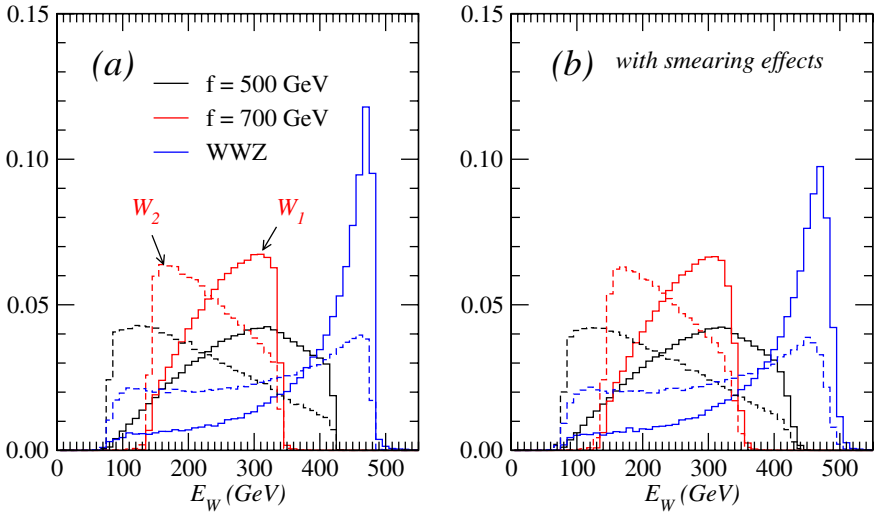

FIG. 13 (color online). Normalized energy distributions of the reconstructed W bosons for $\kappa_q = 1$ at the LC.

In this study, we choose two sample points: (1) $m_{W_H} = 320$ GeV and $m_{A_H} = 66$ GeV for $f = 500$ GeV; (2) $m_{W_H} = 450$ GeV and $m_{A_H} = 101$ GeV for $f = 700$ GeV. Hence, for the former sample point, $E_+ = 426$ GeV and $E_- = 85$ GeV, while for the latter sample point, $E_+ = 345$ GeV and $E_- = 146$ GeV. The small tails of the lower and higher ending points are due to the width effects of W_H and W. After reading out the ending points from the E_W distribution, one can determine m_{W_H} and m_{A_H} from Eqs. (22) and (23). The accuracy of this method highly depends on how well one can reconstruct the W boson momentum and how well one can determine the ending points. Furthermore, the collider detection is not perfect. In order to mimic the finite detection efficiency of the detector, we smear the momenta of all the final state jets by a Gaussian distribution with

$$\frac{\Delta E}{E} = \frac{50\%}{\sqrt{E}}, \tag{24}$$

where E is the energy of the observed parton and the resolution of the energy measurement is assumed to be $50\%\sqrt{E}$. The E_W distributions after energy smearing are shown in Fig. 13(b). We note that the shapes of the distributions of both signal and background are changed slightly, but the positions of the ending points remain almost the same, which lead to 4% and 8% error in the mass measurements of W_H and A_H for $f = 700$ GeV, respectively.

B. Spin correlations

Although one can derive the W_H mass by using E_+ and E_- from the E_W distributions, one still needs to verify that such a signal indeed comes from the LHT and not from other new physics models. For example, the minimal supersymmetric extension of the standard model (MSSM) with R parity can also have exactly the same collider signature ($4j + \not{E}_T$) from the process

$$e^+e^- \to \tilde{W}^+\tilde{W}^- \to \tilde{\gamma}\,\tilde{\gamma}\,W^+(\to jj)W^-(\to jj),$$

where the photino ($\tilde{\gamma}$) is assumed to be the lightest SUSY particle which plays as the dark matter candidate. Obviously, examining the kinematics distributions is not sufficient to discriminate the LHT from the MSSM. Below we will show that the spin correlation between the W boson and its mother particle is a good tool to tell these two models apart. Taking advantage of the known center-of-mass energy of the LC, one can reconstruct the kinematics of the two missing A_H bosons and in turn study the spin correlation effects for model discrimination. Details of the event reconstruction are shown in the appendix. Below, we only present our results of the phenomenological study.

After event reconstruction, we denote A_{H1} as the reconstructed A_H boson associated with W_1 while A_{H2} as the one with W_2. The inequality $\mathbb{C}^2 > 0$ [cf. Eq. (A17)] has to be satisfied in order to reconstruct the momentum of A_H's. Since $\mathbb{C}^2$ depends on m_{W_H} and m_{A_H}, inputting the correct masses of W_H and A_H will significantly enhance the efficiency of the event reconstruction. Furthermore, it is easy to show that the dependence of $\mathbb{C}^2$ upon m_{W_H} is much stronger than the one upon m_{A_H}. Hence, if one inputs the correct m_{W_H}, then one may reach the maximal reconstruction efficiency. The reconstruction efficiencies are summarized in Table II where we consider both cases of with and without detector smearing effects. The detector effects reduce the efficiency of the signal reconstruction about 10% but increase the efficiency of the background reconstruction by a factor $2 \sim 3$.

Using the known kinematics of the A_H bosons, we can reconstruct the momentum of the W_H bosons. We then can plot the $\cos\theta^*$ distribution of the W boson in Fig. 14 where θ^* is the angle between W boson and W_H boson in the rest frame of W_H boson. The left figure shows the true $\cos\theta^*$ distribution where we assume all the particles in the final state, including the A_H bosons, are perfectly tagged. The right figure shows the $\cos\theta^*$ distributions after the W boson reconstruction. The distributions can be understood as follows. In the LHT, the decay products of the W_H boson, W and A_H, are highly boosted because W_H is much heavier than A_H and W. Then the A_H and W bosons would be predominately in the longitudinal polarization states. Therefore, the decay of $W_H \to A_H W$ could be treated as a vector boson decaying into two scalars. Due to the angular momentum conservation, the spacial function of A_H and W_H would be dominated by p-wave ($\sim \sin^2\theta^*$), as shown in Fig. 14(a). Due to the W boson reconstruction, cf. Fig. 13, W_1, the W boson containing the leading jet, moves parallel with the W_H and thus peaks in the forward direction while W_2 peaks in the backward direction.

How could we use this angular correlation to distinguish different models? Let us consider the signature of $W^+W^- + \not{E}_T$ which is generated by two heavy vector bosons in the LHT. That signature could also be induced by many other new physics models:

(i) It can come from the decays of a heavy scalar (Φ) pair, e.g. $e^+e^- \to \Phi\Phi \to W^+W^- + VV$, and the missing particle (V) must be a vector boson. Because of the scalar decay, the $\cos\theta^*$ distribution should be flat, cf. the dotted (red) curve in Fig. 15(a).

(ii) It can also come from the decays of a heavy fermion ($\mathcal{F}$) pair, e.g. $e^+e^- \to \mathcal{F}\mathcal{F} \to W^+W^- + \chi\chi$, and

TABLE II. Efficiencies of the A_H reconstruction after requiring $\mathbb{C}^2 > 0$.

f (GeV)	Input (GeV)		No smearing		With smearing	
	m_{W_H}	m_{A_H}	signal	BKGD	signal	BKGD
500	317	66	87%	0.5%	80%	1.4%
600	384	84	90%	0.3%	82%	0.7%
700	450	101	89%	0.1%	79%	0.3%

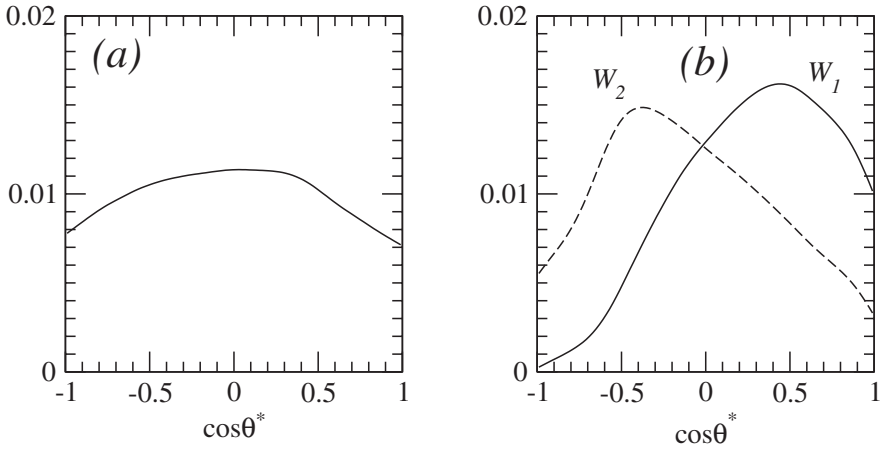

FIG. 14. Normalized distribution of $\cos\theta^*$, where θ^* is the angle between the W boson and its mother particle W_H in the rest frame of W_H for $f = 500$ GeV: (a) true distribution; (b) after the W boson reconstruction.

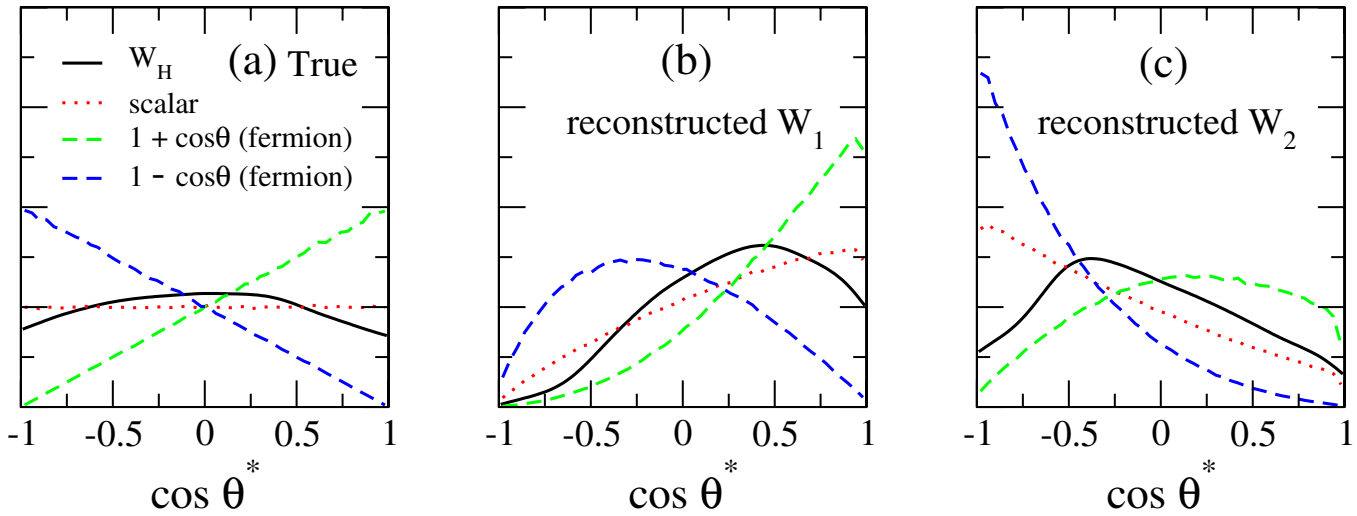

FIG. 15 (color online). Normalized $\cos\theta^*$ distributions for different spin particles: (a) the true distribution while (b) and (c) are the distributions after W boson reconstruction.

the missing particle (χ) must also be a fermion. It is well know that the $\cos\theta^*$ distribution should be in the form of $1 - \cos\theta^*$, $1 + \cos\theta^*$, or the combination of them. Here we plot the first two distributions in Fig. 15(a), cf. the dashed (blue) and dashed (green) curves.[4]

The distinctive difference in the true $\cos\theta^*$ distributions will be affected by the W boson reconstruction, but the predictions from different models are still distinguishable; cf. Fig. 15(b) and 15(c).

[4]We note that the $\cos\theta^*$ distribution is flat if the heavy fermion is unpolarized. It then is impossible to tell Φ and $\mathcal{F}$ apart from the $\cos\theta^*$ distribution. However, the distribution of the W_H pair production in the LHT is still distinguishable from those of Φ and $\mathcal{F}$.

V. CONCLUSION

In this paper we study the collider phenomenologies of the W_H pair production in the LHT at the LHC and the LC. The W_H pair production is of particular importance in the LHT because the mass of W_H is proportional to the symmetry breaking scale f. One thus can unambiguously determine f by measuring m_{W_H}.

At the tree level, the W_H boson pair can be produced either via the s-channel process with the photon and Z boson exchanged or via the t-channel process with a T-odd fermion exchanged. The total cross section highly relies on the mass of the T-odd fermion. Although the s-channel and t-channel contributions are both constructive, their interference effects are destructive. The total cross section reaches the minimum when the s-channel and t-channel contributions are comparable. Once being produced, the W_H boson will decay into a T-odd particle and a T-even

SM particle. The decay pattern of the W_H boson is determined by the masses of other new physics particles such as A_H, ℓ_-, and q_- (we assume A_H being the lightest T-odd particle):

(1) If W_H is the second lightest T-odd particle, it can only decay into $A_H W$.
(2) If W_H is heavier than ℓ_- and/or q_-, it will decay into $\ell\ell_-$ and/or qq_- as well as $A_H W$.

In this work we treat the κ_q and κ_ℓ separately. In order to avoid the flavor changing neutral current problem, we further demand κ_q and κ_ℓ being diagonal in the flavor space.

To avoid the huge QCD background at the LHC, we require the W_H boson decay leptonically. Hence, the signal events can come either from the process in Eq. (11) for $\kappa_\ell = 0.5$ or from the process in Eq. (12) for $\kappa_\ell = 0.3$. We perform a Monte Carlo analysis of the signal process along with the SM backgrounds and find that the W_H boson decaying leptonically, leading to a $\ell^+\ell'^-\not{E}_T$ signature, is very promising at the LHC. We apply the kinematical cuts in Eqs. (13) and (14) and show the resulting significance contour in the plane of κ_q and κ_ℓ in Fig. 10. We find that f can be probed up to 750 GeV for $\kappa_\ell = 0.5$ or 1 TeV for $\kappa_\ell = 0.3$ at the 5σ level with an integrated luminosity of 100 fb^{-1}. It is worth mentioning that f can be probed up to the same limits at the 95% C.L. even at low luminosity ($\mathcal{L} = 10$ fb^{-1}) LHC operation. Although the two processes given in Eqs. (11) and (12) give rise to the exactly same collider signature, they can be further discriminated in the distributions of the transverse momentum and energy of the final state charged leptons, see Fig. 11. However, the W_H boson mass still cannot be determined at the LHC due to the four missing particles in the final state.

In order to determine the mass and spin of the W_H boson, we perform a Monte Carlo study of the W_H pair production at the LC. Owing to the clean background at the LC, we are able to search the W_H boson using its hadronic decay mode which leads to a $4j + \not{E}_T$ signature generated from Eq. (15). Because of the known center-of-mass energy at the LC, the masses of W_H and A_H can be determined from the ending points of the energy distributions of the two reconstructed W bosons. For example, one can measure the mass of W_H (A_H) within an error of 4% (8%) for $f =$ 700 GeV, respectively, even after including the detector smearing effects. Following the study of the W^+W^- pair production at the LEP [44], we present an algorithm of reconstructing the kinematics of two undetectable A_H bosons. It enables us to study the spin correlation between the W boson and its mother particle (W_H) which is a powerful tool to distinguish other new physics models from the LHT, as shown in Fig. 15.

Combining the studies of the $W_H^+W_H^-$ pair production at the LHC and LC, it is possible to determine or further constrain the parameter f, κ_q, and κ_ℓ. In order to fix all the parameters of the LHT, direct search of other independent channels, e.g. top quark partners (both T-odd and T-even) pair production and T-odd fermions (both leptons and quarks) pair production, must be included in a systematic way. One then can compare all these independent channels to check the consistence of the LHT.

ACKNOWLEDGMENTS

We thank Alexander Belyaev, Kazuhiro Tobe, and C.-P. Yuan for useful discussions. Q.-H. Cao is supported in part by the U.S. Department of Energy under Grant No. DE-FG03-94ER40837. C.-R. Chen is supported in part by the U.S. National Science Foundation, No. PHY-0555545.

APPENDIX A: A_H RECONSTRUCTION AT THE LC

In this section we present an algorithm of determining the kinematics of A_H at the LC. This algorithm has been proposed in the study of the W boson at the LEP through the process $e^+e^- \to W^+W^- \to \ell^+\nu_\ell\ell'^-\bar{\nu}_{\ell'}$ [44]. The difficulty is attributed to the existence of two missing particles in the final state. The following kinematics analysis, presented below, shows that the two unobserved momenta of A_H bosons can be determined from the reconstructed W bosons up to a twofold discrete ambiguity, in the limit where the W- and W_H-width are neglected.

Here we consider the process

$$e^+e^- \to AA', \qquad A \to BC, \qquad A' \to B'C', \tag{A1}$$

where $A(A')$ is the mother particle while $B(B')$ and $C(C')$ are the decay products of the mother particles. Here we require $B(B')$ is observable while $C(C')$ undetectable. Furthermore, we assume

$$m_A = m_{A'}, \qquad m_C = m_{C'}. \tag{A2}$$

One of the advantages of the LC is the known center-of-mass energy of the system. For example, the momentum of the incoming particles are

$$p_{e^+} = (E_t, \quad 0, \quad 0, \quad E_t), \tag{A3}$$

$$p_{e^-} = (E_t, \quad 0, \quad 0, \quad -E_t), \tag{A4}$$

where $E_t = \sqrt{S}/2$, where $\sqrt{S}$ is the total energy of the linear collider.

From the momentum conservation, we obtain

$$E_A = E_B + E_C, \qquad E_{A'} = E_{B'} + E_{C'}, \tag{A5}$$

$$\vec{p}_A = \vec{p}_B + \vec{p}_C, \qquad \vec{p}_{A'} = \vec{p}_{B'} + \vec{p}_{C'}, \tag{A6}$$

where $E_i(\vec{p}_i)$ denotes the energy (three momentum) of the particle i, respectively. At the LC,

$$E_A = E_{A'} = E_t, \qquad E_C = E_t - E_B, \qquad E_{C'} = E_t - E_{B'}. \tag{A7}$$

From Eq. (A6) and the on shell conditions of the final state particles we obtain

$$2\vec{p}_B \cdot \vec{p}_C = E_A^2 - m_A^2 - (E_B^2 - m_B^2) - (E_C^2 - m_C^2), \quad \text{(A8)}$$

$$2\vec{p}_{B'} \cdot \vec{p}_{C'} = E_{A'}^2 - m_{A'}^2 - (E_{B'}^2 - m_{B'}^2) - (E_{C'}^2 - m_{C'}^2). \quad \text{(A9)}$$

Using the momentum conservation

$$\vec{p}_B + \vec{p}_{B'} + \vec{p}_C + \vec{p}_{C'} = 0, \quad \text{(A10)}$$

one obtains

$$2\vec{p}_{B'} \cdot \vec{p}_C = (E_{C'}^2 - m_{C'}^2) - (E_{A'}^2 - m_{A'}^2) - (E_{B'}^2 - m_{B'}^2) - 2\vec{p}_B \cdot \vec{p}_B. \quad \text{(A11)}$$

At last, the on shell condition of particle C gives us

$$|\vec{p}_C|^2 = E_C^2 - m_C^2. \quad \text{(A12)}$$

Hence, one can determine $\vec{p}_C$ from Eqs. (A8), (A11), and (A12). We expand $\vec{p}_C$ in term of $\vec{p}_B$ and $\vec{p}_{B'}$ as the following:

$$\vec{p}_C = \mathbb{A}\vec{p}_B + \mathbb{B}\vec{p}_{B'} + \mathbb{C}\vec{p}_B \times \vec{p}_{B'}. \quad \text{(A13)}$$

Then one can derive a and b from Eqs. (A8) and (A11)

$$\begin{pmatrix} \mathbb{A} \\ \mathbb{B} \end{pmatrix} = \frac{1}{|\vec{p}_B|^2|\vec{p}_{B'}|^2 - (\vec{p}_B \cdot \vec{p}_{B'})^2} \times \begin{pmatrix} |\vec{p}_{B'}|^2 & -\vec{p}_B \cdot \vec{p}_{B'} \\ -\vec{p}_B \cdot \vec{p}_{B'} & |\vec{p}_B|^2 \end{pmatrix} \begin{pmatrix} M \\ N \end{pmatrix}, \quad \text{(A14)}$$

where

$$M \equiv \tfrac{1}{2}[E_A^2 - m_A^2 - (E_B^2 - m_B^2) - (E_C^2 - m_C^2)], \quad \text{(A15)}$$

$$N \equiv \tfrac{1}{2}[(E_{C'}^2 - m_{C'}^2) - (E_{A'}^2 - m_{A'}^2) - (E_{B'}^2 - m_{B'}^2) - 2\vec{p}_B \cdot \vec{p}_B]. \quad \text{(A16)}$$

The remaining variable $\mathbb{C}$ is determined using Eq. (A12):

$$\mathbb{C}^2 = \frac{1}{|\vec{p}_B \times \vec{p}_{B'}|^2}[E_C^2 - m_C^2 - \mathbb{A}^2|\vec{p}_B|^2 - \mathbb{B}^2|\vec{p}_{B'}|^2 - 2\mathbb{A}\mathbb{B}\vec{p}_B \cdot \vec{p}_{B'}]. \quad \text{(A17)}$$

The sign of $\mathbb{C}$ cannot be determined. This explicitly exhibits a twofold discrete ambiguity. The inequality $\mathbb{C}^2 > 0$ is expected to be violated only by finite W- and W_H-width effects. Needless to say, using wrong m_C and m_A will lead to a negative $\mathbb{C}^2$ which can serve to measure m_A and m_C as mentioned earlier. In the exceptional case where the momenta of particle B and B' are parallel, one obtains a one-parameter family of solution for which the azimuthal angle of $\vec{p}_C$ with respect to $\vec{p}_B$ is left undetermined.

[1] N. Arkani-Hamed, A. G. Cohen, and H. Georgi, Phys. Lett. B **513**, 232 (2001).
[2] M. Schmaltz and D. Tucker-Smith, Annu. Rev. Nucl. Part. Sci. **55**, 229 (2005).
[3] M. Perelstein, Prog. Part. Nucl. Phys. **58**, 247 (2007).
[4] N. Arkani-Hamed, A. G. Cohen, E. Katz, and A. E. Nelson, J. High Energy Phys. 07 (2002) 034.
[5] C. Csaki, J. Hubisz, G. D. Kribs, P. Meade, and J. Terning, Phys. Rev. D **67**, 115002 (2003).
[6] C. Csaki, J. Hubisz, G. D. Kribs, P. Meade, and J. Terning, Phys. Rev. D **68**, 035009 (2003).
[7] J. L. Hewett, F. J. Petriello, and T. G. Rizzo, J. High Energy Phys. 10 (2003) 062.
[8] M.-C. Chen and S. Dawson, Phys. Rev. D **70**, 015003 (2004).
[9] W. Kilian and J. Reuter, Phys. Rev. D **70**, 015004 (2004).
[10] Z. Han and W. Skiba, Phys. Rev. D **71**, 075009 (2005).
[11] H.-C. Cheng and I. Low, J. High Energy Phys. 09 (2003) 051.
[12] H.-C. Cheng and I. Low, J. High Energy Phys. 08 (2004) 061.
[13] I. Low, J. High Energy Phys. 10 (2004) 067.
[14] J. Hubisz, P. Meade, A. Noble, and M. Perelstein, J. High Energy Phys. 01 (2006) 135.
[15] J. Hubisz and P. Meade, Phys. Rev. D **71**, 035016 (2005).
[16] A. Belyaev, C.-R. Chen, K. Tobe, and C. P. Yuan, Phys. Rev. D **74**, 115020 (2006).
[17] C.-R. Chen, K. Tobe, and C. P. Yuan, Phys. Lett. B **640**, 263 (2006).
[18] S. R. Choudhury, A. S. Cornell, N. Gaur, and A. Goyal, Phys. Rev. D **73**, 115002 (2006).
[19] M. Blanke *et al.*, J. High Energy Phys. 01 (2007) 066.
[20] R. S. Hundi, B. Mukhopadhyaya, and A. Nyffeler, arXiv:hep-ph/0611116.
[21] Q.-H. Cao, C. S. Li, and C. P. Yuan, arXiv:hep-ph/0612243.
[22] M. Blanke *et al.*, J. High Energy Phys. 12 (2006) 003.
[23] M. Blanke *et al.*, Phys. Lett. B **646**, 253 (2007).
[24] M. Blanke, A. J. Buras, B. Duling, A. Poschenrieder, and C. Tarantino, J. High Energy Phys. 05 (2007) 013.
[25] M. Blanke, A. J. Buras, S. Recksiegel, C. Tarantino, and S. Uhlig, arXiv:hep-ph/0703254.

[26] M. Blanke, A. J. Buras, S. Recksiegel, C. Tarantino, and S. Uhlig, J. High Energy Phys. 06 (2007) 082.
[27] S. R. Choudhury, A. S. Cornell, A. Deandrea, N. Gaur, and A. Goyal, Phys. Rev. D **75**, 055011 (2007).
[28] C.-X. Yue and N. Zhang, Europhys. Lett. **77**, 51003 (2007).
[29] C.-S. Chen, K. Cheung, and T.-C. Yuan, Phys. Lett. B **644**, 158 (2007).
[30] H. Hong-Sheng, Phys. Rev. D **75**, 094010 (2007).
[31] P. Kai *et al.*, Phys. Rev. D **76**, 015012 (2007).
[32] L. Wang, W. Wang, J. M. Yang, and H. Zhang, Phys. Rev. D **76**, 017702 (2007).
[33] C.-X. Yue, N. Zhang, and S.-H. Zhu, arXiv:0707.0729.
[34] A. Freitas and D. Wyler, J. High Energy Phys. 11 (2006) 061.
[35] S. Matsumoto, M. M. Nojiri, and D. Nomura, Phys. Rev. D **75**, 055006 (2007).
[36] D. Choudhury and D. K. Ghosh, arXiv:hep-ph/0612299.
[37] M. Carena, J. Hubisz, M. Perelstein, and P. Verdier, Phys. Rev. D **75**, 091701 (2007).
[38] T. Stelzer and W. F. Long, Comput. Phys. Commun. **81**, 357 (1994).
[39] F. Maltoni and T. Stelzer, J. High Energy Phys. 02 (2003) 027.
[40] A. Pukhov, arXiv:hep-ph/0412191.
[41] J. R. Primack, D. Seckel, and B. Sadoulet, Annu. Rev. Nucl. Part. Sci. **38**, 751 (1988).
[42] W. M. Yao *et al.* (Particle Data Group), J. Phys. G **33**, 1 (2006).
[43] K. Kong and S. C. Park, arXiv:hep-ph/0703057.
[44] K. Hagiwara, R. D. Peccei, D. Zeppenfeld, and K. Hikasa, Nucl. Phys. **B282**, 253 (1987).